Composite Structures 247 (2020) 112444

Contents lists available at ScienceDirect

Composite Structures

journal homepage: www.elsevier.com/locate/compstruct

High performance quasi-isotropic thin-ply carbon/glass hybrid composites with pseudo-ductile behaviour loaded off-axis

Mohamad Fotouhi[a,*], Meisam Jalalvand[b], Milad Saeedifar[c], Bill Xiao[d], Michael R. Wisnom[d]

[a] Department of Design and Mathematics, The University of the West of England, Bristol BS16 1QY, UK
[b] Department of Mechanical and Aerospace Engineering, University of Strathclyde, 75 Montrose Street, Glasgow G1 1XJ, UK
[c] Structural Integrity & Composites Group, Faculty of Aerospace Engineering, Delft University of Technology, The Netherlands
[d] Bristol Composites Institute (ACCIS), University of Bristol, Bristol BS8 1TR, UK

ARTICLE INFO

Keywords:
Pseudo-ductility
Hybrid composites
Off-axis
Fragmentation
Acoustic emission

ABSTRACT

The aim of this work was to investigate the effect of loading angle variation on the pseudo-ductility of quasi-isotropic (QI) hybrid composite laminates. Previously, hybrids of thin-ply carbon fibres and standard glass fibres were found to have an excellent pseudo-ductile behaviour both in unidirectional (UD) and QI configurations when subjected to axial tension in the fibres' orientations. In this work, the QI laminates, with 60° intervals, have been subjected to a quasi-static tensile load at various off-axis orientations – i.e. 5°, 10° and 20°. The QI hybrid composites were made by sandwiching a QI T300-carbon laminate between the two halves of a QI S-glass laminate. The results showed a pseudo-ductile behaviour with a linear elastic part and a desirable plateau for all the loading directions, however the pseudo-ductile strain decreases when increasing the off-axis angle. Comparing the 20° off-axis with the other cases, there was more active matrix cracking damage before fragmentation in the 20° off-axis plies and it failed earlier than the other samples. Acoustic emission (AE) results confirmed this, with more matrix cracking related AE signals in the 20° off-axis case compared to the other configurations.

1. Introduction

Advanced composites are frequently used in strength-critical applications where often the direction of loading is unknown, so even if multiple plies are included in a composite plate, it can be loaded off-axis, compared to the direction of its fibres. Previous studies [1,2] demonstrated that due to edge effects, a QI laminate (elastically isotropic in the laminate in-plane) can be highly anisotropic in strength. It was observed that the failure modes change if the loading direction deviates slightly from one of the fibre orientations. These failure modes can combine to produce catastrophic failure and can decrease strength of the composites drastically. In another study [3], the occurrence of damage in a lay-up was studied by examining various orientations of a particular ply without changing the orientation of the others. Matrix cracking was observed in the ply under transverse tension stresses and the laminate elastic moduli underwent changes with crack density.

Recent research publications report on the advantages of using thin-ply laminates [4,5]. Sihn et al. [6] observed that, the thin-ply laminate composites suppress micro-cracking, delamination and splitting damage for static, fatigue and impact loadings. Another interesting work by Guillamet et al. [7], focused on the effect of ply thickness on damage in a QI laminate, under different off-axis uniaxial loadings. In this experimental study, the authors concluded that delamination originating from matrix cracks or free edge effects is delayed or even suppressed in the thin ply laminates.

One of the main disadvantages of high-modulus fibre polymeric based composites is their sudden brittle failure, with linear elastic response and little warning before failure. This drawback leads to the use of large safety factors in design. For example, maximum allowable design strains can be as low as 0.1% for carbon fibre composites, despite maximum fibre failure strains of up to 2% [8–10].

Recent studies investigated the use of different types of fibres in hybrid composites to introduce gradual failure and prevent sudden brittle failure in composites materials. For that reason, UD [11–13], and multidirectional [14,15] hybrids combining high strain fibres (such as glass) and low strain fibres (such as carbon) with different combinations of thin and standard ply thickness prepregs, were introduced which can generate a nonlinear stress-strain response and pseudo-ductility that avoids catastrophic failure. In addition, orientation-dispersed QI composite plates with sublaminates of the different materials blocked together showed a desirable pseudo-ductility when loaded in all the fibres orientations and avoided free-edge delamination [16]. The

* Corresponding author.

https://doi.org/10.1016/j.compstruct.2020.112444
Received 5 April 2020; Received in revised form 20 April 2020; Accepted 1 May 2020
Available online 07 May 2020

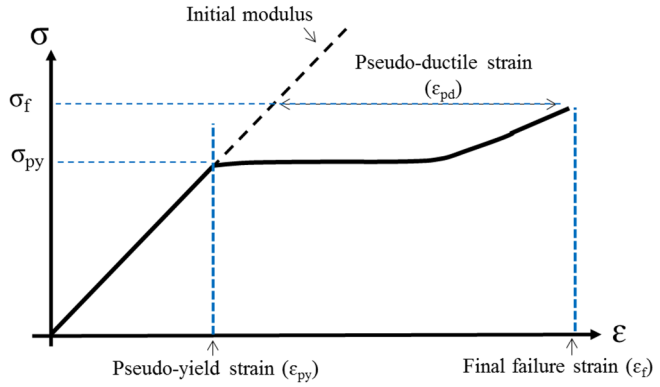

Fig. 1. Schematic of the stress–strain graph of a thin-ply hybrid with pseudo-ductility.

Table 1
Characteristics of the prepregs and fibres applied.

Prepreg type	S-glass/epoxy [12]	USN020A (T300/epoxy) [11]
Fibre modulus E (GPa)	88	230[b]
Fibre failure strain (%)	5.5	1.5
Cured nominal thickness (mm)	0.155	0.029
Fibre mass per unit area (g/m^2)	190	21
Fibre volume fraction (%)	50.0	40.5
E1 (GPa)	45.7	101.7
E2 (GPa)	15.4[a]	6.0[c]
G12 (GPa)	4.34[a]	2.40[c]
V12	0.3[a]	0.3[c]
Equivalent in-plane stiffness for QI (GPa)	15.2	37.8

[a] Assumed to be equal to E-glass properties used in Ref. [24].
[b] This value is based on T300 Data Sheet [25].
[c] The transverse properties were assumed to be equal to the similar USN020A prepreg utilised in Ref. [26], as the data was not available.

failure mechanisms in the pseudo-ductile hybrid composites are influenced by the material properties, thickness of the layers, and the interfacial toughness. When the low strain layer is thin enough, catastrophic delamination propagation following the first low strain layer fracture is suppressed and further fractures in the low strain layer occur. This damage mode was called fragmentation of the low strain layer. Fig. 1 shows the failure process of the pseudo-ductile laminates with three different damage modes of low strain materials fragmentation, delamination and high strain material failure. The pseudo-yield strain (ε_{py}) is the maximum strain level during the initial linear elastic behaviour and the final failure strain is the maximum strain that the high strain material can achieve before the composite's final fracture. The pseudo-ductile strain (ε_{pd}) is calculated as the difference between the final failure strain (ε_f), and the elastic strain based on the initial modulus at the final failure stress, which is the enhancement in strain due to the gradual failure.

These UD and QI hybrid composite laminates showed excellent pseudo-ductility when subjected to tensile loads quasi-statically, in fatigue [17], and at high strain rates [18], through fragmentation and stable pull-out of the low strain layers.

However, the development of damage mechanisms in pseudo-ductile QI hybrid laminates with off-axis loading has not yet been investigated. This is of great importance as the activated failure modes in off-axis loading, matrix-cracking and free edge delaminations, can combine to produce catastrophic and unstable failure such as shear out [1] and can decrease strength of the composites drastically by hindering or overtaking the pseudo-ductile damage modes, i.e. fragmentation and dispersed delamination.

Acoustic Emission (AE) is an efficient method for on-line and continuous monitoring of damage mechanisms in laminated composites. AE signals originate from the sudden release of strain energy due to damage formation inside the material. It was reported by many researchers that AE technique can characterise the damage modes in laminated composites [19,20]. Cumulative AE counts and AE energy curves were used by previous researchers for identification of thresholds for damage evolution during loading [21,22]. In previous studies, the AE method was successfully used to detect damage initiation and to characterise the failure mechanisms in pseudo-ductile UD carbon-S-glass/epoxy [23] and QI all-carbon/epoxy [14] hybrid laminates under tensile loading. The AE event characteristics (amplitude and energy) were associated with fragmentation of carbon plies and delamination of the glass/carbon interface.

This paper presents a novel investigation carried out on the behaviour of pseudo-ductile QI hybrids under off-axis tensile loading conditions. QI specimens from an orientation-dispersed QI hybrid composite plate fabricated from thin-ply T300-Carbon/S-glass epoxy hybrid laminates were loaded in all the fibre directions and off-axis directions (0°, 5°, 10° and 20°). The results showed that these hybrids can generate pseudo-ductility when loaded in tension in the off-axis orientations as well as the all fibre orientations. AE monitoring confirmed the existence of the pseudo-ductile failure modes, i.e. fragmentation and dispersed delamination, however more matrix cracking related AE signals were observed with increasing off-axis angle. The activated matrix-cracking in the off-axis loading did not hinder the pseudo-ductile failure modes, however it decreased the strength of the composites for the 20° off-axis loading.

2. Design and experimental procedures

2.1. Materials and specimen design

Material properties of the utilised prepregs are reported in Table 1. The high strain material is standard thickness UD S-glass/913 epoxy prepreg supplied by Hexcel and the low strain material is thin carbon prepreg (SkyFlex USN020A) from SK Chemicals (South Korea) that has T300 carbon fibres made by Toray. The corresponding matrix was SK Chemical's type K 50 epoxy resin. The resin systems in the hybrid laminates were 120 °C curing epoxies. Although no details were provided by the suppliers on the chemical formulation of the resins, good integrity of the hybrid laminates was confirmed during test procedures and no phase separation was observed on cross sectional micrographs.

Table 2
Layups of the investigated laminates.

Specimen type	Resulting layup
0° axis	$[60_{S\text{-glass}}/-60_{S\text{-glass}}/0_{S\text{-glass}}/0_{C\text{-T300}}/60_{C\text{-T300}}/-60_{C\text{-T300}}]_s$
60° axis = 0° axis + 60°	$[-60_{S\text{-glass}}/0_{S\text{-glass}}/60_{S\text{-glass}}/60_{C\text{-T300}}/-60_{C\text{-T300}}/0_{C\text{-T300}}]_s$
−60° axis = 0° axis + 60°	$[0_{S\text{-glass}}/60_{S\text{-glass}}/-60_{S\text{-glass}}/-60_{C\text{-T300}}/0_{C\text{-T300}}/60_{C\text{-T300}}]_s$
0° off-axis	$[60_{S\text{-glass}}/-60_{S\text{-glass}}/0_{S\text{-glass}}/60_{C\text{-T300}}/-60_{C\text{-T300}}/0_{C\text{-T300}}]_s$
5° off-axis = Ref + 5°	$[65_{S\text{-glass}}/-55_{S\text{-glass}}/5_{S\text{-glass}}/65_{C\text{-T300}}/-55_{C\text{-T300}}/5_{C\text{-T300}}]_s$
10° off-axis = Ref + 10°	$[70_{S\text{-glass}}/-50_{S\text{-glass}}/10_{S\text{-glass}}/70_{C\text{-T300}}/-50_{C\text{-T300}}/10_{C\text{-T300}}]_s$
20° off-axis = Ref + 20°	$[80_{S\text{-glass}}/-40_{S\text{-glass}}/20_{S\text{-glass}}/80_{C\text{-T300}}/-40_{C\text{-T300}}/20_{C\text{-T300}}]_s$

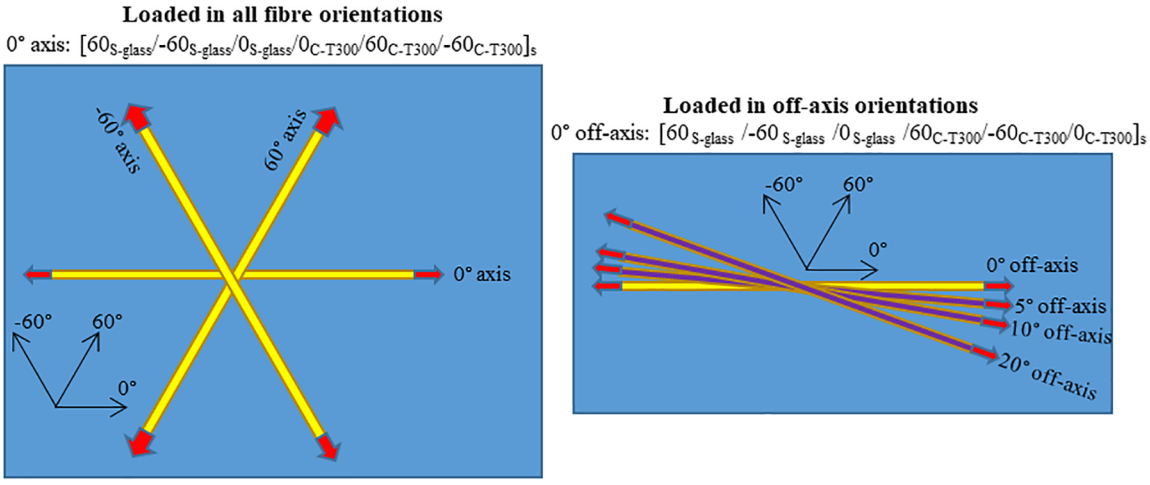

Fig. 2. Schematic of the investigated laminates in a QI composite plate, the red arrows showing the loading directions.

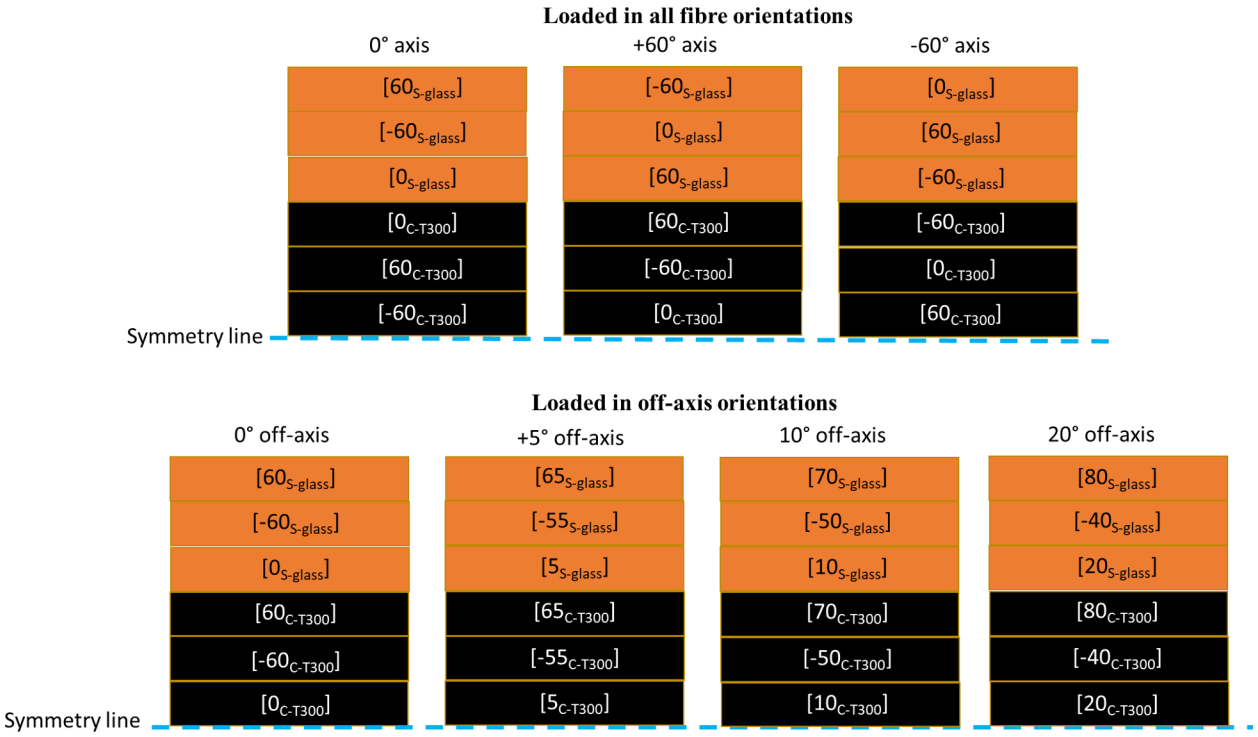

Fig. 3. Schematic of the investigated layups.

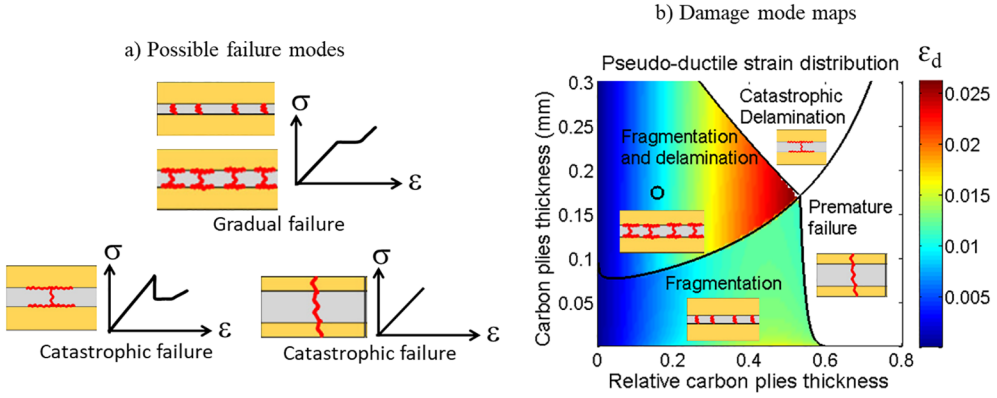

Fig. 4. a) Possible failure modes in a three layer hybrid composite, b) Distribution of pseudo-ductile strain for the investigated specimens loaded in fibre orientations. Carbon plies thickness is the thickness of the homogenised carbon layers (0.174 mm = 6 plies with 0.029 mm as each ply thickness). Relative carbon plies thickness is the ratio of the carbon plies thickness to the overall thickness of the laminate.

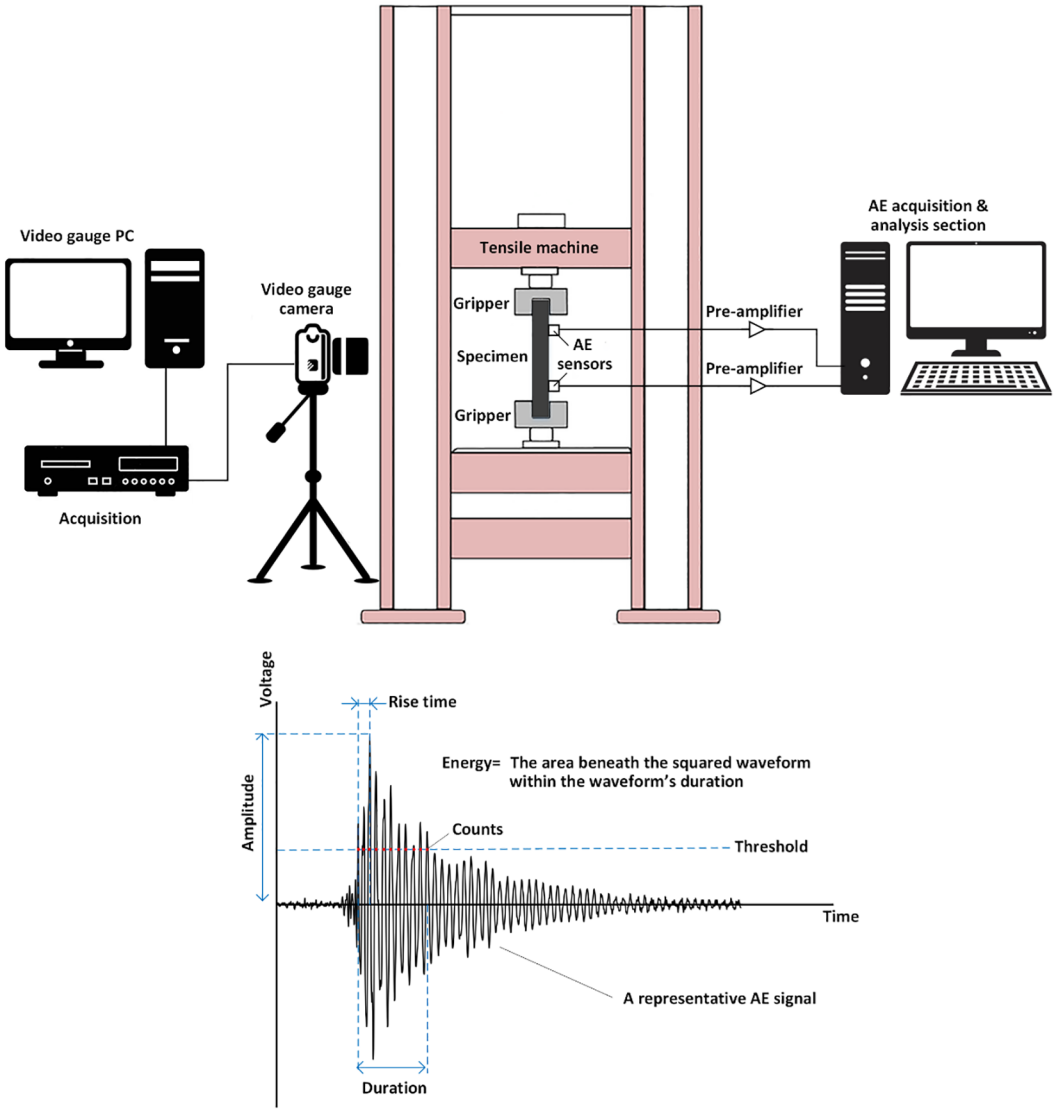

Fig. 5. Schematic of the experimental setup, and the definitions for acoustic-emission parameters.

Table 2 gives information about the hybrid specimen types and the sequences in which they were laid up. From Table 2 and as shown in Figs. 2 and 3, adding the specified angles to the orientation of each sub-laminate, produces the other QI layups, with the 0° direction defined as the loading direction.

The specimens were designed using the damage mode map, which shows how the failure mode depends on the thickness and proportion of carbon plies [12]. The damage mode map was generated for predicting the damage sequence based on the order of the required stresses for each damage mode. The investigated hybrid layups were chosen to be in the Fragmentation and dispersed Delamination (Frag. & Del.) region to get the desired damage scenario (see Fig. 4). The damage mode maps were obtained by homogenising the multi-directional glass and carbon sub-laminates before crack development. Cracks are assumed to propagate through the thickness of the whole carbon epoxy sublaminate. More details regarding damage mode map calculations can be found in our previous work [16].

The reason for different layups in the 0° axis and 0° off-axis laminates is because the tests were done at two different times. Initially the 0° axis, +60° axis and −60° axis laminates were fabricated and tested, and at the time it was thought that the 0° axis layup is the optimum layup for a QI hybrid configuration [16]. However, in this case the ply orientations were not evenly distributed, for example 0° carbon and 0° glass plies are adjacent in the 0° axis layup. So, a new lay-up, as illustrated for the 0° off-axis laminate, was selected for the second set of experiments to better disperse the ply orientations. The new layup is believed to result in a uniform property distribution of the hybrid laminates.

2.2. Specimen manufacturing

The laminates were cured in an autoclave at the recommended cure temperature and pressure cycle for the Hexcel 913 resin (60 min at 125 °C, 0.7 MPa), which was also satisfactory for the resin of the carbon plies. Specimens were cut using a diamond-cutting wheel. End tabs made of 2 mm thick woven glass/epoxy plates supplied by Heathcote Industrial Plastics Ltd. were bonded to the specimens using a two component Araldite 2000 A/B epoxy adhesive supplied by Huntsman, the components were mixed with the volume fraction ratio of 100: 50 for A: B respectively and cured for 120 min at 80 °C inside a Carbolite oven. The nominal specimen dimensions were 240/160/20/h mm overall length/free length/width/variable thickness respectively.

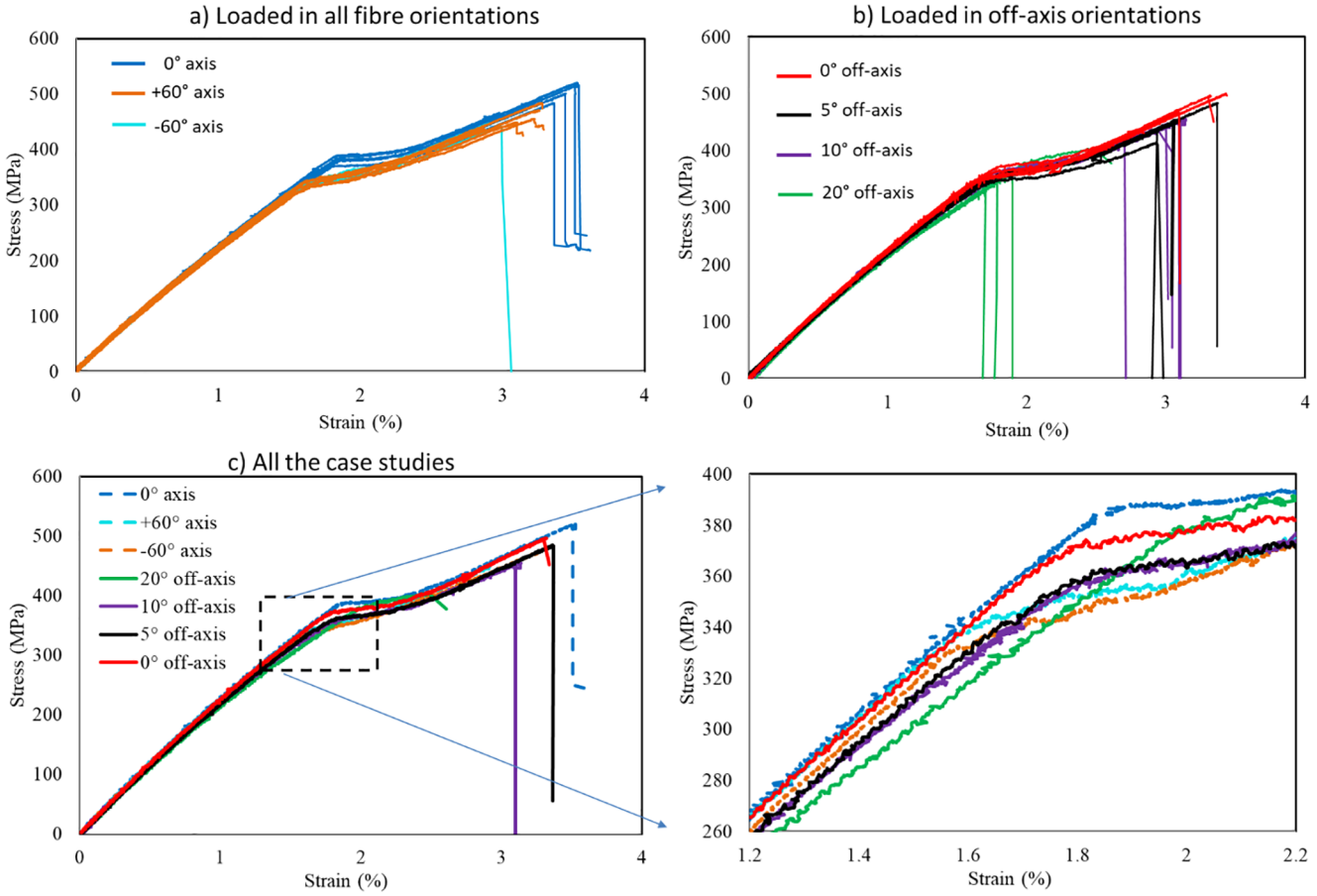

Fig. 6. Results of the tensile tests for, a) all the samples, b) a representative sample from each configuration.

Table 3
Summary of the test results.

Specimen type	Pseudo-yield strain (%)	Fibre direction strain at "yield"	Pseudo-ductile strain (%)	Max-stress (MPa)	Initial modulus (GPa)
0° axis	1.80 ± 0.02	1.80 ± 0.02	1.30 ± 0.05	504 ± 18	23.5 ± 0.1
+60° axis	1.60 ± 0.04	1.60 ± 0.04	1.15 ± 0.10	436 ± 14	23.1 ± 0.2
−60° axis	1.60 ± 0.02	1.60 ± 0.02	1.20 ± 0.06	464 ± 16	23.2 ± 0.1
0° Off-axis	1.76 ± 0.06	1.76 ± 0.06	0.91 ± 0.14	473 ± 32	22.8 ± 0.2
5° Off-axis	1.72 ± 0.05	1.70 ± 0.05	0.83 ± 0.07	456 ± 26	23.1 ± 0.3
10° Off-axis	1.73 ± 0.01	1.66 ± 0.01	0.77 ± 0.04	442 ± 5	23.5 ± 0.3
20° Off-axis	1.97	1.67	0.30	366 ± 16	22.4 ± 0.6

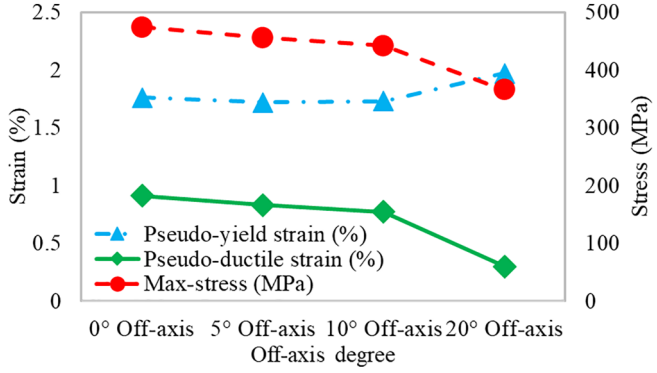

Fig. 7. Comparison of the results for different off-axis degrees.

2.3. Test procedure

Tensile testing of the hybrid laminates was performed under uni-axial loading and displacement control using a crosshead speed of 2 mm/min on a computer controlled Instron 8801 type 100 kN rated universal hydraulic test machine with wedge-type hydraulic grips. A 25 kN load cell was used for better resolution in the expected load range. At least 6 specimens of each type were tested to check the repeatability of the results. To measure the strains over a nominal gauge length of 130 mm, an Imetrum video gauge system was used by tracking a dotted pattern applied on the specimen face.

2.4. AE device

The AE signals were recorded with a PAC PCI-2 acoustic emission

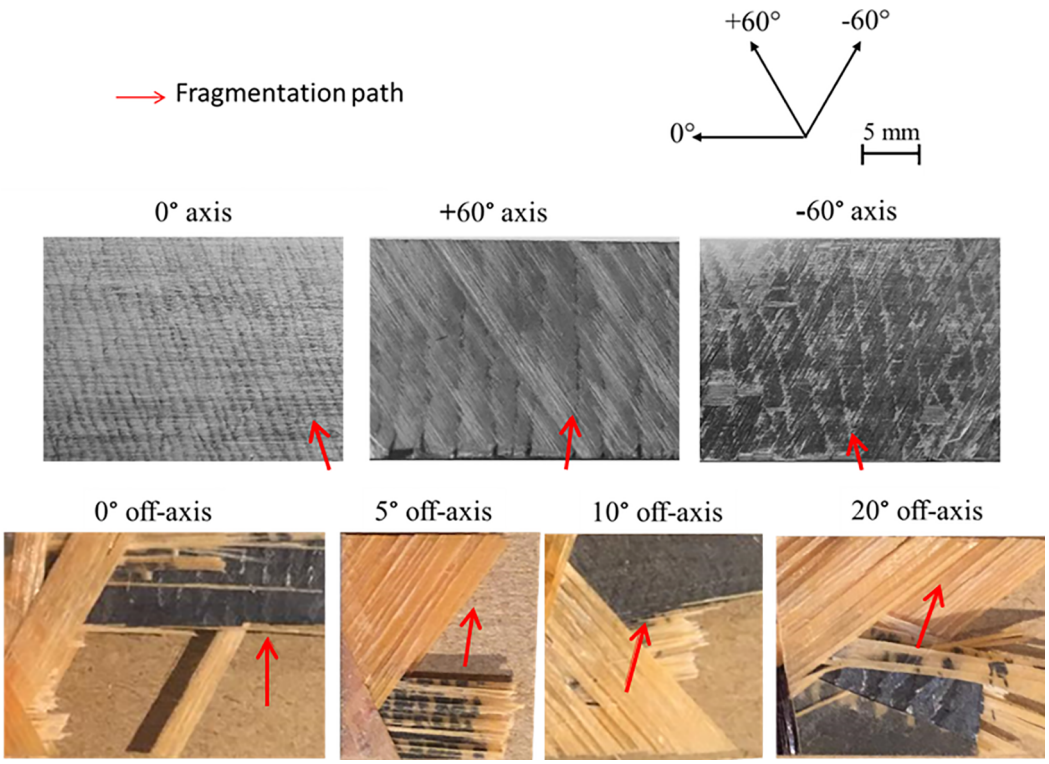

Fig. 8. Fragmentation pattern in the carbon layer over the whole width of the investigated layups. For the 0° axis, +60° axis and −60° axis samples the pictures were taken from the carbon layers with the top glass layers removed, however for the off-axis samples, the pictures were taken from the broken specimens without removing any layers.

device at a 5 MHz sampling rate using two WSA type 100–1000 kHz wideband sensors attached to the specimens with clips and silicone grease as an acoustic coupler. The gain selector of the preamplifier and the threshold value were set to 40 dB. A pencil lead break procedure was used to calibrate the data acquisition system for each of the specimens. After the calibration step, the AE signals were recorded during the tests as illustrated in Fig. 5.

3. Results and discussion

3.1. Overall mechanical results

Fig. 6 shows stress-strain response of the investigated laminates. The desired pseudo-ductile response was achieved with all curves showing smooth transitions between the initial linear part and an obvious plateau. The carbon plies started to fragment near the knee-point. Along the plateau stable progressive carbon ply fragmentation and local delamination of the carbon fragments occurred. The investigated configurations, except the 20° off-axis case, continued to fragment and witnessed the second linear part, where the glass plies carried most of the increase in the load. For the 20° off-axis configuration, the specimens failed shortly after the start of fragmentation, except one sample that was tested without the end tabs and showed a plateau.

Table 3 gives some of the important features of the curves such as the initial elastic modulus, pseudo-yield strain, pseudo-ductile strain and maximum stress of these hybrid configurations. Pseudo-yield strain values were defined as the intersection of two lines fitted to the stress-strain graphs before and after the fragmentation initiation point. Fibre direction strain at "yield" values were estimated using the transformation of strains (Eq. (1)), considering $\gamma_{xy} = 0$. The angle between the loading direction and the fibre direction is called the $\theta_{off-axis}$. The transverse strain was calculated from the measured laminate Poisson's ratio (0.3) times the longitudinal strain, which is valid since the in-plane properties are quasi-isotropic.

$$\varepsilon_{off-axis} = \frac{1}{2}(\varepsilon_{longitudinal} + \varepsilon_{transverse}) + \frac{1}{2}(\varepsilon_{longitudinal} - \varepsilon_{transverse})\cos 2\theta_{off-axis} + \frac{\gamma_{xy}}{2}\sin 2\theta_{off-axis} \quad (1)$$

Fig. 7 shows trends of these features with increasing off-axis angle. The elastic response, i.e. initial modulus of the layups is the same, as expected; however, by increasing the off-axis angle, there is more matrix cracking in the glass plies and consequently there is more non-linearity for the higher degrees of off-axis angle, as observable from Fig. 6(c). From Fig. 7, there is a decreasing trend for the pseudo-ductile strain and maximum stress by increasing the off-axis angle. An increase was observed for the pseudo-yield strain when increasing the off-axis angle from 10° to 20°. This needs further investigation. For the 20° off-axis configuration, the pseudo-yield strain is calculated for the single specimen that experienced the plateau.

The failure mechanisms for the tested samples in each batch were not identical, but their damage sequence and pattern were similar. Fig. 8 shows the appearance of the fragmentations in the carbon plies for one sample of each condition for all the investigated samples after the final failure, confirming the pseudo-ductile failure modes. Fig. 9 illustrates the off-axis tested specimens after failure and for all the case studies except the 20° off-axis, the specimens failed in the gauge length. For the 20° off-axis case, there was significant matrix cracking in the glass plies, and this may have increased the stress concentration near the end tabs, leading to premature failure from the tabs. A similar phenomenon has been previously reported for quasi-isotropic tension tests where specimens were found to have higher strengths when tested

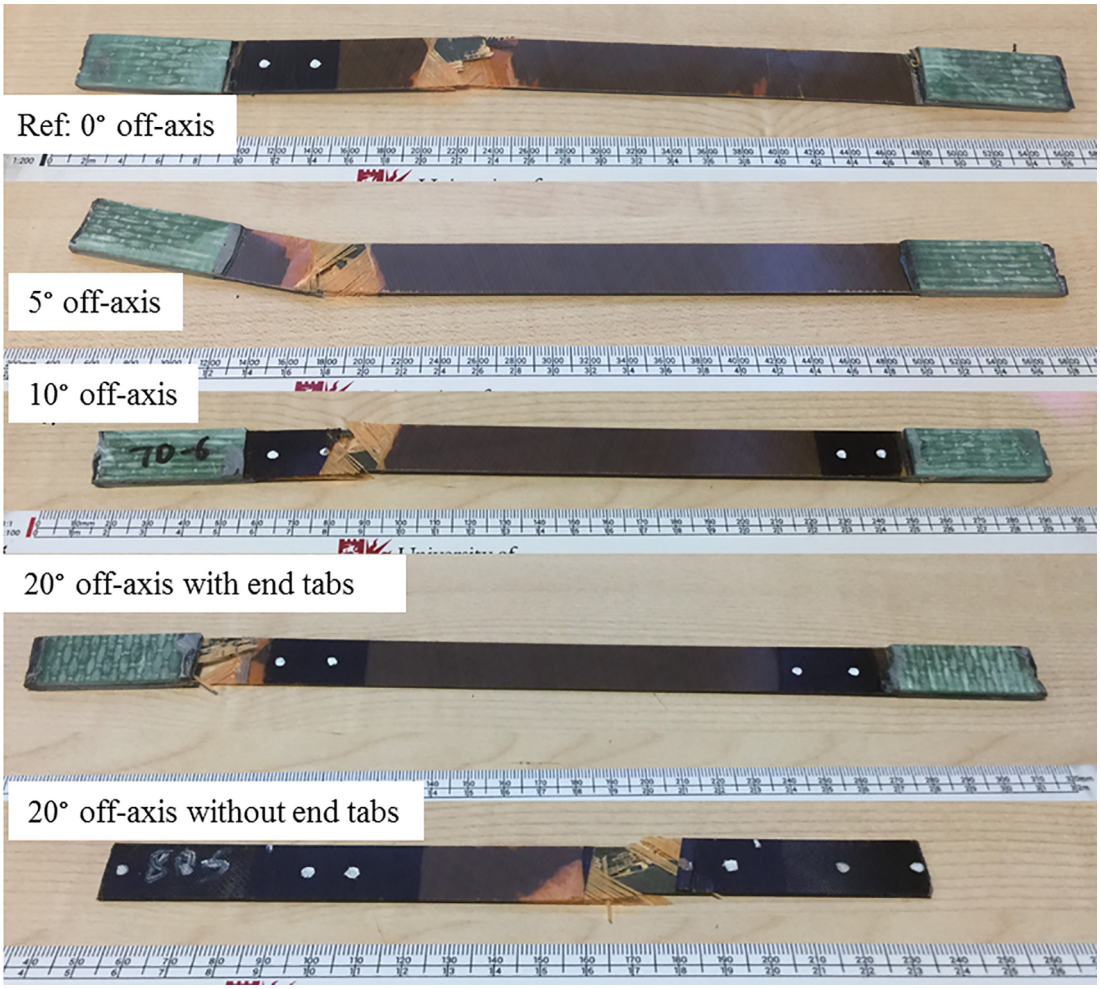

Fig. 9. Comparison between the final failures of the investigated samples.

without end tabs [27]. Unlike the other 20° off-axis specimens, the 20° off-axis specimen that was tested without the end tabs showed a gauge length failure as is observable from Fig. 9.

3.2. Acoustic emission results

Recording AE events during the tests helped to get more information about the failure mechanism. Previous studies reported that it is possible to characterize the mechanisms by studying the energy and the amplitude of the events during the failure [23]. It was concluded that higher energies represent fibre failure or fragmentations, whereas medium and lower values are mostly in connection with delamination and matrix cracking.

The recorded AE energy and cumulative energy results from the investigated specimens are illustrated in the same diagrams as the stress values against strain (see Fig. 10). There are peaks of energy resulted from the fragmentation of the carbon layers which behaved like a brittle failure and released a proportionately large amount of energy in a short time. There are different AE pattern distributions for different specimens due to the difference in their failure modes. From the diagrams (Figs. 10 and 11) it can be seen that there are more active AE signals for the 20° off-axis specimen starting from 1% strain into the test. Comparing the energy level of the AE signals near the knee-point, the energy level for the 20° off-axis is lower than the other samples showing more matrix cracking related AE signals in the 20° off-axis and more fragmentation related AE signals for the other configurations. The rise of the cumulative AE energy, as shown in Fig. 11, indicates significant damage appearance in the specimens. Table 4 shows strain levels at which there was significant rise of the cumulative AE energy in the specimens. This reflects the existence of glass ply matrix-cracking in the off-axis loading cases at strain levels lower than the fragmentation strain. The matrix cracks had a small effect for the 10° off-axis and 5° off-axis loading, whereas they decreased the strength for 20° off-axis loading (see Table 3).

4. Conclusions

This paper investigated the effect of loading angle variation, (i) along the different fibre orientations, i.e. 0°, 60°, −60°, and (ii) at different off-axis orientations – i.e. 5°, 10° and 20°, on the pseudo-ductility of QI hybrid composite laminates, consisting of thin-ply carbon T300/standard thickness S-glass prepregs, and the following conclusions are drawn:

- A pseudo-ductile behaviour with a linear elastic part and a desirable plateau was achieved for all the loading directions, however the pseudo-ductile strain decreases with increasing off-axis angle.
- Shear out failures from the free edge were not observed for any of

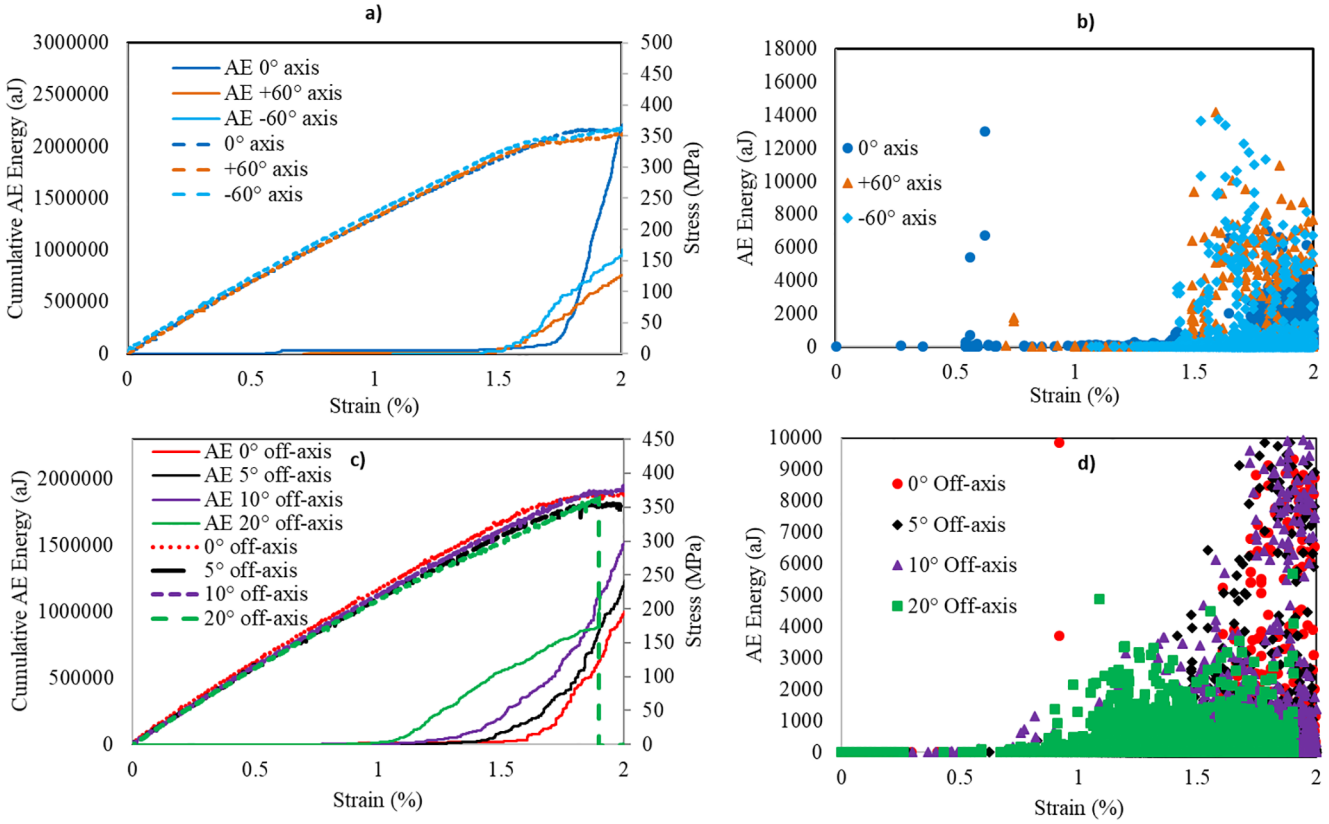

Fig. 10. Cumulative AE energy-strain versus the stress-strain (a, d) and AE Energy-strain (b, c) for the investigated samples.

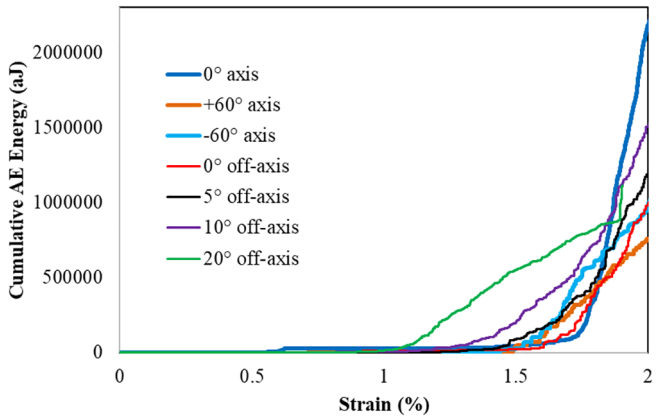

Fig. 11. Cumulative AE energy-strain for the investigated samples.

the loading angles. Fragmentation of the carbon plies was observed for all the loading directions.

- For the 20° off-axis samples with end tabs, the pseudo-ductility did not develop, and the material failed with brittle behaviour. This is due to the existence of more matrix cracking damage in the 20° off-axis case, compared to the 0°, 5° and 10° samples, which caused stress concentration in the end tabs and this laminate failed earlier than the others. Testing the 20° off-axis sample without the end tabs, a desirable plateau but no secondary linear part was observed.
- Overall, by increasing the off-axis angle, the elastic response, i.e. initial modulus of the layups is unchanged, however, there is a decreasing trend for the pseudo-ductile strain and maximum stress.
- AE monitoring detected earlier damage initiation with increasing off-axis angle and can explain the brittle behaviour of the 20° off-axis case due to higher active matrix cracking damage in this case compared to the others.

Declaration of Competing Interest

The authors declare that they have no known competing financial interests or personal relationships that could have appeared to influence the work reported in this paper.

Table 4
Strain levels at which there was significant rise of the cumulative AE energy.

Specimen type	0° axis	+60° axis	−60° axis	0° Off-axis	5° Off-axis	10° Off-axis	20° Off-axis
Strain level (%)	1.75	1.55	1.55	1.60	1.50	1.30	1.10

Acknowledgements

This work was funded under the UK Engineering and Physical Sciences Research Council (EPSRC) Programme Grant EP/I02946X/1 on High Performance Ductile Composite Technology in collaboration with Imperial College, London. The authors acknowledge Hexcel Corporation for supplying glass fibre material for this research. The data necessary to support the conclusions are included in the paper.

References

[1] Sun CT, Zhou S. Failure of quasi-isotropic composite laminates with free edges. J Reinf Plast Compos 1988;7(6):515–57.
[2] Sun CT, Jen KC. On the effect of matrix cracks on laminate strength. J Reinf Plast Compos 1987;6:208–22.
[3] Varna J, Akshantala NV, Talreja R. Damage in composite laminates with off axis plies. Compos Sci Technol 1999;59:2139–47.
[4] Arteiro A, Furtado C, Catalanotti G, Linde P, Camanho PP. Thin-ply polymer composite materials: a review. Compos Part A Appl Sci Manuf 2020;132:105777. https://doi.org/10.1016/j.compositesa.2020.105777.
[5] Galos J. Thin-ply composite laminates: a review. Compos Struct 2020;236:111920https://doi.org/10.1016/j.compstruct.2020.111920.
[6] Sihn S, Kim R, Kawabe K, Tsai S. Experimental studies of thin-ply laminated composites. Compos Sci Technol 2007;67(6):996–1008.
[7] Guillamet G, Turon A, Costa J, Renart J, Linde P, Mayugo JA. Damage occurrence at edges of non-crimp-fabric thin-ply laminates under off-axis uniaxial loading. Compos Sci Technol 2014;98(27):44–50.
[8] Byers BA. Behavior of damaged graphite/epoxy laminates under compression loading. Seattle, WA: Boeing Commercial Airplane Co; 1980.
[9] Sanchez-Saez S, Barbero E, Zaera R, Navarro C. Compression after impact of thin composite laminates. Compos Sci Technol 2005;65(13):1911–9. https://doi.org/10.1016/j.compscitech.2005.04.009.
[10] Cantwell WJ, Morton J. The impact resistance of composite materials – a review. Composites 1991;22:347–62. https://doi.org/10.1016/0010-4361(91)90549-V.
[11] Czél G, Wisnom MR. Demonstration of pseudo-ductility in high performance glass-epoxy composites by hybridisation with thin-ply carbon prepreg. Compos Part A Appl Sci Manuf 2013;52:23–30. https://doi.org/10.1016/j.compositesa.2013.04.006.
[12] Jalalvand M, Czél G, Wisnom MR. Damage analysis of pseudo-ductile thin-ply UD hybrid composites – a new analytical method. Compos Part A Appl Sci Manuf 2014;69:83–93. https://doi.org/10.1016/j.compositesa.2014.11.006.
[13] Czél G, Jalalvand M, Wisnom MR. Design and characterisation of advanced pseudo-ductile unidirectional thin-ply carbon/epoxy–glass/epoxy hybrid composites. Compos Struct 2016;143:362–70. https://doi.org/10.1016/j.compstruct.2016.02.010.
[14] Czél G, Rev T, Jalalvand M, Fotouhi M, Longana ML, Nixon-Pearson OJ, et al. Pseudo-ductility and reduced notch sensitivity in multi-directional all-carbon/epoxy thin-ply hybrid composites. Compos Part A Appl Sci Manuf 2018;104:151–64. https://doi.org/10.1016/j.compositesa.2017.10.028.
[15] Fuller JD, Jalalvand M, Wisnom MR. Combining fibre rotation and fragmentation to achieve pseudo-ductile CFRP laminates. Compos Struct 2016;142:155–66. https://doi.org/10.1016/j.compstruct.2016.01.073.
[16] Fotouhi M, Jalalvand M, Wisnom MR. High performance quasi-isotropic thin-ply carbon/glass hybrid composites with pseudo-ductile behaviour in all fibre orientations. Compos Sci Technol 2017;152:101–10. https://doi.org/10.1016/j.compscitech.2017.08.024.
[17] Suwarta P, Fotouhi M, Czél G, Longana M, Wisnom MR. Fatigue behaviour of pseudo-ductile unidirectional thin-ply carbon/epoxy-glass/epoxy hybrid composites. Compos Struct 2019;224:110996. https://doi.org/10.1016/j.compstruct.2019.110996.
[18] Fotouhi M, Fuller J, Longana M, Jalalvand M, Wisnom MR. The high strain rate tension behaviour of pseudo-ductile high performance thin ply composites. Compos Struct 2019;215:365–76. https://doi.org/10.1016/j.compstruct.2019.02.068.
[19] Bohse J. Acoustic emission characteristics of micro-failure processes in polymer blends and composites. Compos Sci Technol 2000;60(8):1213–26.
[20] International A. ASTM E976–10, Standard guide for determining the reproducibility of acoustic emission sensor response. West Conshohocken, PA: ASTM International; 2010.
[21] Suresh Kumar C, Arumugam V, Dhakal HN, John R. Effect of temperature and hybridisation on the low velocity impact behavior of hemp-basalt/epoxy composites. Compos Struct 2015;125:407–16.
[22] Saeedifar M, Fotouhi M, Najafabadi MA, Toudeshky HH. Prediction of delamination growth in laminated composites using acoustic emission and cohesive zone modeling techniques. Compos Struct 2015;124:120–7.
[23] Fotouhi M, Suwarta P, Jalalvand M, Czel G, Wisnom MR. 2016 Detection of fibre fracture and ply fragmentation in thin-ply UD carbon/glass hybrid laminates using acoustic emission. Compos Part A Appl Sci Manuf 2016;86:66–76. https://doi.org/10.1016/j.compositesa.2016.04.003.
[24] Hallett SR, Wisnom MR. Numerical investigation of progressive damage and the effect of layup in notched tensile tests. J Compos Mater 2005;40:1229–45.
[25] T300 Data Sheet - No. CFA-001, http://www.toraycfa.com/pdfs/T300DataSheet.pdf; n.d.
[26] Fuller J, Wisnom MR. Damage suppression in thin ply angle-ply carbon/epoxy laminates. In: 19th Int. conf. compos. mater. Montreal, http://confsys.encs.concordia.ca/ICCM19/AllPapers/FinalVersion/FUL80507.pdf; 2013.
[27] Xu X, Wisnom MR, Chang K, Hallett SR. Unification of strength scaling between unidirectional, quasi-isotropic, and notched carbon/epoxy laminates. Compos Part A Appl Sci Manuf 2016;90:296–305. https://doi.org/10.1016/j.compositesa.2016.07.019.